PERGAMON

International Journal of Solids and Structures 37 (2000) 1873–1897

INTERNATIONAL JOURNAL OF SOLIDS and STRUCTURES

www.elsevier.com/locate/ijsolstr

Cohesive element modeling of viscoelastic fracture: application to peel testing of polymers

P. Rahulkumar[a], A. Jagota[b,*], S.J. Bennison[b], S. Saigal[a]

[a]*Department of Civil and Environmental Engineering, Carnegie Mellon University, Pittsburgh, PA 15213, USA*
[b]*CR&D, The DuPont Company, Experimental Station, Wilmington, DE 19880-0356, USA*

Received 23 May 1998; in revised form 18 November 1998

Abstract

A computational modeling technique for fracture propagation in viscoelastic materials using cohesive elements for the zone ahead of the crack tip is presented. The computational technique is used to study the problem of increase in fracture energy with peel velocity in peel testing of polymers. A rate-independent phenomenological cohesive zone model is used to model the intrinsic fracture toughness of the interface between the polymer sheets. A dimensional analysis reveals that the macroscopic fracture energy scales with the intrinsic fracture toughness and is a function of peel velocity, and parameters such as the thickness, bulk properties of the polymer sheets, and other cohesive zone properties. The growth of fracture energy as a function of the peel velocity has been studied for polymer sheets characterized by a standard linear viscoelastic solid. Viscoelastic losses in the peel arm vanish in the limits of very slow and rapid peeling. Peak dissipation is obtained at an intermediate velocity, which is related to the characteristic relaxation time and thickness. This behavior is interpreted in terms of the size of elastic and viscous zones near the crack tip. It is found that the total energy dissipated is dependent upon both the intrinsic fracture toughness and the characteristic opening displacement of the cohesive zone model. The computational framework has been used to model experimental data on peeling of Butadiene rubbers. It is found that the usual interpretation of these data, that the macroscopic dissipation equals the *rate-independent* intrinsic toughness multiplied by a factor that depends on rate of loading, leads to a large quantitative discrepancy between theory and experiment. It is proposed that a model based on a rate-dependent cohesive law be used to model these peel tests.

Keywords: Fracture; Cohesive zone models; Finite elements; Cohesive elements; Peel tests; Viscoelasticity; Polymers; Fracture energy; Rubber

1. Introduction

The use of polymers in structural design requires an understanding of the conditions that lead to their

* Corresponding author. Fax: 001-302-695-1664.
E-mail address: anand.jagota@usa.dupont.com (A. Jagota)

0020-7683/00/$ - see front matter
PII: S0020-7683(98)00339-4

failure by initiation and growth of cracks over time. For deformations over a range of temperatures above the glass transition temperature, the mechanical behavior of amorphous polymers can often be characterized using viscoelastic theories. Several researchers have contributed to the present day knowledge of fracture initiation and propagation in viscoelastic materials. Williams (1963), Knauss (1973), and Schapery (1975) developed theories for macroscopic cracks propagating in a linear viscoelastic continuum. These are based on the presence of a cohesive zone near the crack tip that is a continuum representation of material degradation and failure at a microscopic level by one of many possible mechanisms. Such cohesive zone models were originally proposed by Dugdale (1960) and Barenblatt (1962) for fracture in rate-insensitive materials. Williams (1963) derived the conditions for crack initiation in a linear Voigt solid based on the assumption of an average critical strain in the material at the crack tip. It was assumed that the stress ahead of the crack tip reaches a constant peak value over a certain length and that the crack initiates once the strain in this region reaches a critical value. Knauss (1973) developed a theory for constant rates of crack propagation in a linear viscoelastic material. The stress transmitted within the cohesive zone was approximated by a rate-independent bilinear cohesive stress-opening displacement relationship. Two possible criteria, one based on an ultimate crack opening displacement, and another based on critical energy were proposed for crack propagation in the macroscopic viscoelastic continuum. Schapery (1975) developed a similar theory for transient crack propagation in a linear isotropic viscoelastic medium. No explicit assumptions about the stress-opening displacement relationship that characterizes the cohesive zone were made. An energy based crack propagation criterion was proposed, and the theory is applicable to both constant and varying crack propagation velocities of the crack tip.

It has been recognized that, depending on the physical nature of the fracture process, the stress that the crack tip-specific cohesive zone carries may be rate-dependent (Hui et al., 1992; Knauss, 1993). However, in most early works, a rate-independent cohesive zone representing the intrinsic work of fracture has been used satisfactorily to model experimental data. Moreover, it has been argued that the intrinsic fracture toughness of rubbers is rate-independent and on the order of 20–50 J/m^2 (Lake and Thomas, 1967), and that the difference between measured and intrinsic fracture toughness can be attributed to viscoelastic losses in the bulk (Kinloch, 1987; Gent, 1996).

In recent studies on viscoelastic fracture Knauss and Losi (1993), instead of specifying an explicit function for the cohesive stresses, use a nonlinear viscoelastic material model for the cohesive zone. In the limit of small strains the nonlinear viscoelastic model is identical to the linear viscoelastic model used to describe the bulk. De Gennes (1996, 1997) presented a theoretical picture of various zones near a crack tip propagating in a weakly cross-linked viscoelastic solid. The concept of a 'viscoelastic trumpet', which represents the various zones around a propagating crack tip, was introduced to explain the scaling and growth in the fracture energy with crack velocity. Fig. 1 depicts the viscoelastic trumpet comprising of three distinct zones along with the cohesive zone at the propagating crack tip. In an infinite specimen, these three zones are: (1) the unrelaxed zone characterized by the small time modulus of the material, G_0; (2) a surrounding viscous dissipation zone which contributes to the bulk dissipation in the material; and (3) an exterior zone that is fully relaxed characterized by the long time modulus, G_∞. For a crack propagating in an infinite viscoelastic medium it is shown that the macroscopic fracture energy scales with the intrinsic cohesive energy, consistent with most previous theoretical and experimental work. The size of the viscous dissipation zone, and thus the volume of the material in the viscous dissipation zone, grows with increasing crack velocity. For a crack propagating in a finite viscoelastic specimen the size of the viscous dissipation zone is limited by the specimen thickness. Then, fracture energy increases with increasing velocity, attains a peak, and decreases for further increase in velocity. Hui et al. (1992) studied crack propagation along the interface of two semi-infinite polymer sheets. Using small scale yielding assumptions, and a linear solid viscoelastic model for the bulk, they found that the macroscopic fracture toughness scales with the intrinsic fracture toughness of the

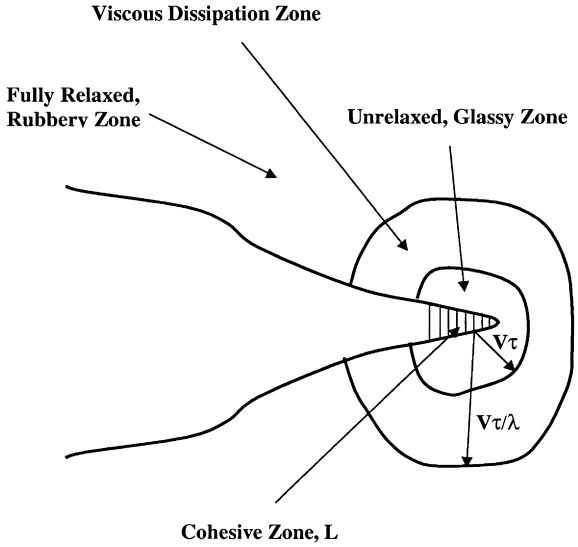

Fig. 1. Schematic drawing depicting different zones around a crack propagating with velocity, V, in a viscoelastic material with $\lambda = G_\infty/G_0$ and a characteristic relaxation time, τ (de Gennes, 1996; Hui et al., 1992).

interface. It grows without bound with increasing crack propagation velocity. Xu et al. (1992) have extended this analysis to study a steadily moving crack along the interface between two finite-size polymer specimens. They find that with increasing velocity the macroscopic fracture energy grows to a peak, and subsequently falls back to the intrinsic fracture energy of the interface as predicted by De Gennes (1996, 1997).

The inclusion of a cohesive zone introduces a length scale even for crack propagation in an infinite specimen. As a consequence, it is not necessary that all three of de Gennes' regions exist; at slow rates the glassy and viscous regions may be smaller than the cohesive zone. This fact leads to a seeming discrepancy between the cohesive zone and energy flux approach to fracture of viscoelastic materials, as pointed out by Rice (1978). As is well known (Rice, 1978; Lawn, 1993), the cohesive zone and critical energy release rate models for crack propagation are fully consistent for elastic–brittle materials if the size of the cohesive zone, L, is much smaller than the crack length, a, or any other characteristic dimension in the problem. However, Rice (1978) has shown that there is an inconsistency between the sharp, featureless view of the crack tip and one based on a cohesive zone of finite dimensions, in the limit of small crack velocities. This is when the glassy and viscous regions become smaller than the cohesive zone size. Hence, a successful continuum model for crack growth in viscoelastic materials requires some coupling of the fracture process occurring in the finite size cohesive zone and the bulk deformation.

In this paper we develop a computational framework using cohesive zone models for fracture in viscoelastic materials. We use it to study a model problem of peel testing of polymer adhesives. A study of peel testing is important in its own right as it is a well-established experimental test used to characterize the strength of adhesives. Macroscopic fracture energy in a peel test, measured by the peel force, combines the intrinsic interfacial fracture energy and viscous dissipation in the peel arm. Several investigators (Gent and Petrich, 1969; Andrews and Kinloch, 1973; Ahagon and Gent, 1975; Gent and Hamed, 1977; Chang and Gent, 1981; Gent and Lai, 1994; Gent, 1996) have studied experimentally the effect of peeling rate on the measured peel strength of viscoelastic polymer adhesives. For a fixed failure mode, peel energy typically increases with rate of peeling, v, and can vary by more than three orders of

magnitude. At low velocities and high temperatures, it approaches a lower limit asymptotically; this is usually identified as the intrinsic toughness of the interface. The experimentally measured fracture toughness, Γ, is found to be described well by an empirical relation of the form

$$\Gamma = \Gamma_0\left[1 + f(a_T v, T_r)\right] \tag{1}$$

where Γ_0 is the intrinsic fracture energy of the interface, a_T is the WLF (Williams, Landel, Ferry) shift function for a polymer (Ferry, 1980), and T_r is a reference temperature. In the peeling of polymer adhesives from stiff substrates one often finds a transition from cohesive to adhesive failure accompanied by a sudden decrease in peel energy (Gent and Petrich 1969; Derail et al., 1997). The function $f(a_T v, T_r)$ in eqn (1) represents the irreversible viscous energy dissipated in the peel arm as a function of reduced rate of peeling, $a_T v$. Peel fracture energies exhibit time–temperature superposition characteristic of viscoelastic processes. The values of Γ_0 are estimated by performing the peel experiments at low rates and high temperatures, conditions under which viscoelastic dissipation is minimal. The values of Γ_0 so estimated range from 10 to 50 J/m^2. That these values are large compared to surface energy due to breakage of primary bonds (≈ 2 J/m^2) has been explained by a model which assumes that all the stored elastic energy between cross-links is lost in the fracture process (Lake and Thomas, 1967). The intrinsic fracture energy, Γ_0, is usually interpreted as a rate-independent number representative of bond strength. A rate-dependent intrinsic cohesive zone can equally well satisfy the form eqn (1), as long as its parameters obey time–temperature superposition (Xu et al., 1992).

Several analyses of viscoelastic peel and related tests have been performed. The studies of Kendall (1972), Aravas et al. (1989), and Loukis and Aravas (1991) assume the peel shape at steady state in the form of a root angle as it joins the substrate. The fracture energy is computed from the evaluated peel shape for a given root angle using beam theory. The total dissipation in the analysis is assumed to be equal to the sum of the intrinsic strength of the interface, Γ_0, and viscous dissipation in the peel arm. Although this additive decoupling does not preclude a dependence of viscous dissipation on Γ_0, it does hide the generally accepted multiplicative coupling between intrinsic and macroscopic fracture energy for viscoelastic fracture. A similar analysis for peeling of elastic–plastic materials has been performed by Kinloch et al. (1994). Analyses of related tests that include a cohesive zone have been presented recently by Xu et al. (1992), Knauss (1993), and Knauss and Losi (1993). There appear to be no computational analyses of the peel test for viscoelastic materials in the literature that include a cohesive zone as part of the model.

In this paper we present the development of a computational methodology within an implicit finite element framework to model crack propagation in viscoelastic materials accounting for the cohesive zone that represents the fracture process at the crack tip. Specifically, we seek to explore, using this computational framework, the relationship between macroscopic and intrinsic fracture energy, and the effect of cohesive zone parameters on these predictions. The numerical modeling of the cohesive zone is based on the use of cohesive elements. The computational model is used to analyze a model peel test of a standard linear viscoelastic solid. The effect on the predicted fracture toughness of the various parameters characterizing the cohesive zone model is investigated. Finally we model the experimental peel test of Gent (1996) on Butadiene rubbers using their measured viscoelastic properties and intrinsic fracture toughness.

2. Computational model formulation

The computational model consists of the bulk material modeled as a continuum along with a cohesive zone for the fracture process at the crack tip. The bulk material is modeled using standard

displacement-based finite elements, and the cohesive zone is modeled using cohesive elements. The cohesive element approach employed here is similar to that used by Needleman (1990), Tvergaard and Hutchinson (1992), Xu and Needleman (1994), and Camacho and Ortiz (1996) for studying fracture in elastic–plastic and brittle solids. Similar elements have been used to model fracture in concrete by Bocca et al. (1991), Gerstle and Xie (1992), and Bazant and Planas (1998).

The principle of virtual work for the bulk material and cohesive zone is given as

$$\int_V \sigma{:}\delta\mathbf{d}\,\mathrm{d}V + \int_S \mathbf{T}\cdot\delta\dot{\Delta}\frac{1}{J}\mathrm{d}S - \int_A \mathbf{F}\cdot\delta\mathbf{v}\,\mathrm{d}A = 0 \tag{2}$$

where: σ is the Cauchy stress tensor; $\delta\mathbf{d}$ is the virtual rate of deformation tensor; $\mathbf{T}$ is the vector of cohesive tractions; Δ is the vector of displacement jumps across the cohesive surfaces; $\mathbf{F}$ is the vector of externally applied tractions; $\delta\mathbf{v}$ is the vector of the virtual velocity field; V is the current volume of the bulk material; S is the current internal surface area over which the cohesive forces are acting; A is the current external surface area over which the external tractions are applied; J is the Jacobian of the transformation between the current deformed and original undeformed areas of the cohesive surfaces. The surface area over which the virtual work of the cohesive tractions is integrated corresponds to the original undeformed area, S^0, not the current area, S, as represented by the deformed cohesive element. The latter would be customary in an updated Lagrangian finite element framework. By evaluating the virtual work integral over the initial unstretched configuration of the cohesive element, we ensure that the work of separation associated with this unit area is independent of the in-plane stretch of the element. This is appropriate for modeling fracture in solids for which it may be assumed that the number of bonds broken are fixed per unit undeformed area, S^0, of crack surface formed (Lake and Thomas, 1967). For liquids, it would be more appropriate to define fracture energy based on current area.

An implicit finite element solution for the unknown displacement configuration for a given set of loads requires the evaluation of the first variation of the virtual work equation. This results in the tangent stiffness matrix needed for Newton–Raphson iterations. The implementation of cohesive elements then requires the evaluation of the first variation for the second term of eqn (2). This virtual work of the cohesive forces is given as

$$\delta W_{\mathrm{c}} = \int_s \left(\delta\dot{\Delta}_{\mathrm{n}} T_{\mathrm{n}} + \delta\dot{\Delta}_{\mathrm{t}} T_{\mathrm{t}}\right)\frac{1}{J}\mathrm{d}S \tag{3}$$

where T_{n} and T_{t} are the normal and tangential tractions respectively, and $\delta\dot{\Delta}_{\mathrm{n}}$ and $\delta\dot{\Delta}_{\mathrm{t}}$ are the normal and tangential jump velocities across the cohesive zone surface. Substituting the virtual jump velocities in terms of the cohesive element nodal shape functions and the nodal virtual jump velocities, the discretized virtual work in the current configuration, $\delta\bar{W}_{\mathrm{c}}$, is obtained as

$$\delta\bar{W}_{\mathrm{c}} = \int_s \left(\delta\dot{\bar{\Delta}}_{\mathrm{n}}^{\mathrm{T}}\mathbf{N}^{\mathrm{T}} T_{\mathrm{n}} + \delta\dot{\bar{\Delta}}_{\mathrm{t}}^{\mathrm{T}}\mathbf{N}^{\mathrm{T}} T_{\mathrm{t}}\right)\frac{1}{J}\mathrm{d}S \tag{4}$$

where the bar denotes cohesive element nodal values, the superscript T denotes a transpose operation, and $\mathbf{N}$ is the vector of cohesive element nodal shape functions. The form of eqn (4) ensures that the virtual work so integrated can be used with bulk finite elements that are formulated using an updated Lagrangian formulation. The first variation of the virtual work, $\mathrm{d}\delta\bar{W}_{\mathrm{c}}$, is given as

$$\mathrm{d}\delta\bar{W}_{\mathrm{c}} = \int_s \left(\delta\dot{\bar{\Delta}}_{\mathrm{n}}^{\mathrm{T}}\mathbf{N}^{\mathrm{T}}\,\mathrm{d}T_{\mathrm{n}} + \delta\dot{\bar{\Delta}}_{\mathrm{t}}^{\mathrm{T}}\mathbf{N}^{\mathrm{T}}\,\mathrm{d}T_{\mathrm{t}}\right)\frac{1}{J}\mathrm{d}S + \int_s \left(\delta\dot{\bar{\Delta}}_{\mathrm{n}}^{\mathrm{T}}\mathbf{N}^{\mathrm{T}} T_{\mathrm{n}} + \delta\dot{\bar{\Delta}}_{\mathrm{t}}^{\mathrm{T}}\mathbf{N}^{\mathrm{T}} T_{\mathrm{t}}\right)\mathrm{d}\left(\frac{1}{J}\right)\mathrm{d}S \tag{5}$$

where dT_n, dT_t are the incremental normal and tangential tractions, respectively. In eqn (5) the second term accounts for the stretching of the cohesive element. For small stretching of the cohesive element this term is negligible and the first variation of the virtual work can be approximated as

$$d\delta\bar{W}_c \approx \int_s \left(\delta\dot{\bar{\Delta}}_n^T \mathbf{N}^T\, dT_n + \delta\dot{\bar{\Delta}}_t^T \mathbf{N}^T\, dT_t\right)\frac{1}{J}dS \tag{6}$$

which is the form we use. Incremental tractions are related to incremental jump velocities by the cohesive material Jacobian, $[C]$, as

$$\begin{Bmatrix} dT_n \\ dT_t \end{Bmatrix} = [C]\begin{Bmatrix} d\dot{\Delta}_n \\ d\dot{\Delta}_t \end{Bmatrix} \tag{7}$$

$$[C] = \begin{bmatrix} \dfrac{\partial T_n}{\partial \Delta_n} & \dfrac{\partial T_n}{\partial \Delta_t} \\ \dfrac{\partial T_t}{\partial \Delta_n} & \dfrac{\partial T_t}{\partial \Delta_t} \end{bmatrix} \tag{8}$$

Substituting the incremental tractions in terms of the incremental jump velocities from eqn (7) into eqn (6), and writing the incremental jump velocities in terms of the incremental cohesive element nodal velocities, the tangent stiffness matrix takes the form

$$K_T = \int_s [A]^T[C][A]\frac{1}{J}dS \tag{9}$$

where $[A]$ is the matrix of cohesive element nodal shape functions that relates the nodal velocities to the velocities of the displacement jumps within the cohesive element. The stiffness matrix implemented using eqn (9) gives an approximate tangent for Newton–Raphson iterations. However, no approximation is made in computing tractions, and hence equilibrium is ensured upon convergence.

The constitutive law for an isotropic viscoelastic bulk material for small strains and rotations is given by the hereditary integral

$$\sigma(t) = \sigma_0(t) + \int_0^t \left(\frac{\dot{G}(t')}{G_0}\mathbf{S}_0(t-t') + \mathbf{I}\frac{\dot{K}(t')}{K_0}p_0(t-t')\right)dt' \tag{10}$$

where t is the current time; G_0 and K_0 are instantaneous small strain shear and bulk moduli respectively; $\mathbf{S}_0$ and p_0 are the deviatoric and hydrostatic components, respectively, of the instantaneous Cauchy stress, σ_0; and $\mathbf{I}$ is the second order identity tensor. A superposed dot implies differentiation with respect to time. A generalization of the above hereditary integral for the deformation state of a material point in a peel test characterized by small strains and large rotations is given as

$$\sigma(t) = \sigma_0(t) + \left[\int_0^t \mathbf{R}_t^T(t-t') \cdot \left(\frac{\dot{G}(t')}{G_0}\mathbf{S}_0(t-t') + \mathbf{I}\frac{\dot{K}(t')}{K_0}p_0(t-t')\right) \cdot \mathbf{R}_t(t-t')dt'\right] \tag{11}$$

where $\mathbf{R}_t(t-t')$ is the material point rotation tensor that rotates the configuration at time t' to the configuration at current time t. This generalization can be interpreted as rotating the stress at some previous time $(t-t')$, into the current configuration of the material point at time, t, in order to satisfy the principle of objectivity of stress. For a situation characterized by large strains and large rotations the

deformation gradient, $\mathbf{F}_t(t-t')$, is used in place of $\mathbf{R}_t(t-t')$. For the deformation state of the material in a peel test we have $\mathbf{F} \approx \mathbf{R}$ (Ogden, 1984).

For computational convenience, the bulk relaxation modulus, $K(t)$, and shear relaxation modulus, $G(t)$, are represented by a generalized Maxwell series as

$$K(t) = K_\infty + \sum_{i=1}^{n_K} K_i \exp\left(-\frac{t}{\tau_i^K}\right) \quad G(t) = G_\infty + \sum_{i=1}^{n_G} G_i \exp\left(-\frac{t}{\tau_i^G}\right) \tag{12}$$

where K_∞ and G_∞ are long term bulk and shear moduli, respectively. The material is assumed to have different relaxation times, τ_i^K and τ_i^G, for bulk and shear relaxation, respectively, and the corresponding bulk and shear moduli are given as K_i and G_i. The number of generalized series terms n_K and n_G, for bulk and shear behavior, respectively, need not be the same.

The phenomenological cohesive law of Xu and Needleman (1994) has been used to represent the intrinsic fracture zone. It is rate-independent and relates the tractions acting across cohesive surfaces to their respective displacement jumps using a potential function, ϕ. It has been pointed out that the detailed shape of the cohesive law is relatively unimportant (Knauss, 1973; Rice, 1978). The two independent parameters that characterize the cohesive law are important: Γ_0 and δ_{cr}, the energy of separation per unit area and a characteristic opening displacement. The potential function for the Xu and Needleman (1994) potential is given as

$$\phi(\Delta_n, \Delta_t) = \phi_n + \phi_n \exp\left(-\frac{\Delta_n}{\delta_n}\right)\left\{\left[1 - r + \frac{\Delta_n}{\delta_n}\right]\frac{1-q}{r-1} - \left[q + \left(\frac{r-q}{r-1}\right)\frac{\Delta_n}{\delta_n}\right]\exp\left(-\frac{\Delta_t^2}{\delta_t^2}\right)\right\} \tag{13}$$

where δ_n and δ_t are the critical normal and tangential openings, respectively, of the cohesive zone. Normal and tangential forces in the cohesive zone decrease in magnitude once the corresponding normal and tangential relative displacements exceed these critical values. ϕ_n and ϕ_t are the works or fracture energies of normal and tangential separation, and the parameters q and r are given as

$$q = \frac{\phi_t}{\phi_n}, \quad r = \frac{\Delta_n^*}{\delta_n} \tag{14}$$

where Δ_n^* is the value of Δ_n after complete shear separation for $T_n = 0$. Tractions are derived from the potential function, ϕ, as

$$T_n = -\frac{\partial \phi}{\partial \Delta_n}, \quad T_t = -\frac{\partial \phi}{\partial \Delta_t} \tag{15}$$

This potential-based model allows for different normal and tangential works of separation. The ability to derive tractions using eqn (15) allows for a continuous specification of tractions along the cohesive zone. The material Jacobian of the cohesive elements as given by eqn (8), which is required in the formulation of the tangent stiffness matrix for these elements, can be derived by differentiating the tractions given by eqn (15) with respect to the normal and tangential openings. The material Jacobian so obtained is a smooth and continuous function of the openings, a highly desirable feature for Newton–Raphson iterations in an implicit finite element framework.

The normal fracture energy, ϕ_n, and the tangential fracture energy, ϕ_t, can be written in terms of the cohesive surface normal strength, σ_{max}, and tangential strength, τ_{max}, as

$$\phi_n = e\sigma_{max}\delta_n, \quad \phi_t = \sqrt{\frac{e}{2}}\tau_{max}\delta_t \tag{16}$$

where e = exp(1). In all analyses presented here we assume that the cohesive zone has identical normal and tangential fracture energies, and identical normal and tangential critical opening displacements. Thus: $\phi_n = \phi_t = \Gamma_0; \delta_n = \delta_t = \delta_{cr}; q = 1$. The value of r in eqn (14), is taken as zero. For these parameters the potential simplifies to

$$\phi(\Delta_n, \Delta_t) = \Gamma_0 \left[1 - \left(1 + \frac{\Delta_n}{\delta_{cr}} \right) \exp\left(- \frac{\Delta_n}{\delta_{cr}} \right) \exp\left(- \frac{\Delta_t^2}{\delta_{cr}^2} \right) \right] \tag{17}$$

The above computational model formulation for cohesive elements has been implemented as a family of 2D and 3D cohesive elements for use with implicit static and implicit dynamic procedures in the general-purpose finite element code ABAQUS® (1997) using the user defined routines. The cohesive zone model implementation is independent of the kinematics of the cohesive elements. Hence any other cohesive zone model implemented in this library is available to all of the 2D and 3D cohesive elements for use with static and dynamic procedures. This element library can be used to study fracture initiation and propagation along with various bulk finite elements using different material models.

3. Verification of the computational framework

3.1. Elastic double cantilever problem

The problem of a crack propagating along an elastic double cantilever beam (DCB) as shown in Fig. 2 is used to verify the cohesive element implementation. A two-dimensional plane strain large deformation analysis is performed. Due to symmetry about the x-axis, only one half of the double cantilever is modeled. A schematic of the finite element mesh used in the DCB analysis is shown in Fig. 3. The spring and beam element shown in the Figure are not used in the DCB analysis and are used in the peel analysis described later. The cantilever beam is modeled with four-node bulk plane-strain elements with incompatible mode shape functions that help alleviate mesh locking in bending. The crack grows and propagates along the x-axis to the right, and cohesive elements are placed along the x-axis to model this crack growth. Linear, four-node, cohesive elements are used in the analysis. The cohesive elements have a top and a bottom face with two nodes on each face. The top faces of the cohesive elements are attached to the adjacent bulk plane strain elements. In the undeformed configuration the top and bottom faces of the cohesive elements, as well as the corresponding nodes, are coincident. As the load is applied, the bulk elements deform and thereby pull the top face of the cohesive elements away from the bottom face.

Symmetry boundary conditions are specified by constraining displacement in the y-direction and tractions along x-direction to be zero for all the nodes on the bottom face of the cohesive elements along the x-axis. The nodes on the top face of the cohesive elements are constrained to have the same displacement in the x-direction as the corresponding nodes on the bottom face. Nodes on the face at

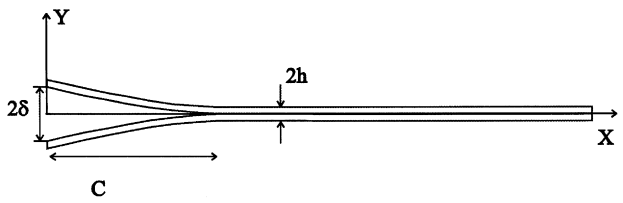

Fig. 2. Crack in an elastic double cantilever beam (DCB).

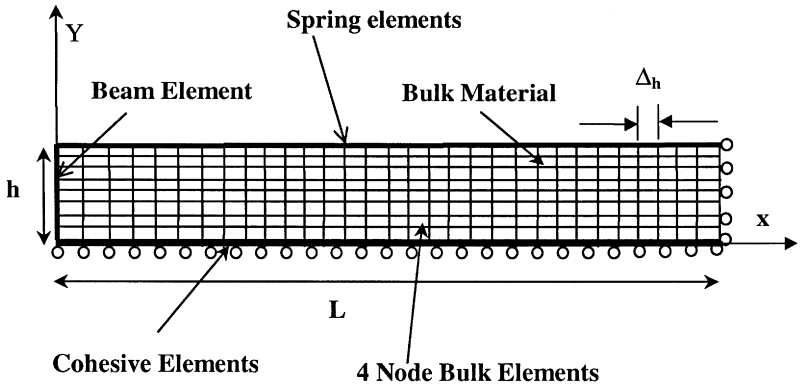

Fig. 3. Schematic drawing of the finite element mesh for DCB, and elastic and viscoelastic peel analyses.

$x = L$ are constrained to have displacement $u_x = 0$. Loading consists of an applied displacement, δ, to the node located at $x = 0$, $y = 0$. A uniform mesh with each cohesive element of size Δ_h, Fig. 3, has been used in the analysis. The material is characterized by the parameters: Young's modulus, $E = 100$ GPa; Poisson ratio, $v = 0.25$. Cohesive zone properties are: fracture energy $\Gamma_0 = \phi_n = \phi_t = 1.0 \times 10^6$ J/m^2; critical opening displacements, $\delta_{cr} = \delta_n = \delta_t = 1.0 \times 10^{-2}$ m. The length (L) and thickness (h), Fig. 3, of the beam modeled in this analysis are 100.0 m, and 1.0 m, respectively. A normalized cohesive element size, $\Delta_h/\delta_{cr} = 12.5$, has been used. The crack tip is defined as the location along the x-axis where the normal opening in the cohesive elements equals the critical opening displacement, δ_{cr}. Cracks in the DCB specimen grow stably under the above boundary and loading conditions, which allows a quasi-static analysis. A plot of the calculated crack length, c, normalized with the peel thickness, h, versus the normalized crack opening displacement, δ/δ_{cr}, along with the analytical relation for the crack length and crack opening displacement (Lawn, 1993) is shown in Fig. 4. The cohesive element results are in good agreement with analytical predictions based on linear elastic fracture mechanics (LEFM) theory. The DCB figure shown in Fig. 2 is the actual deformed shape plot of the model analyzed.

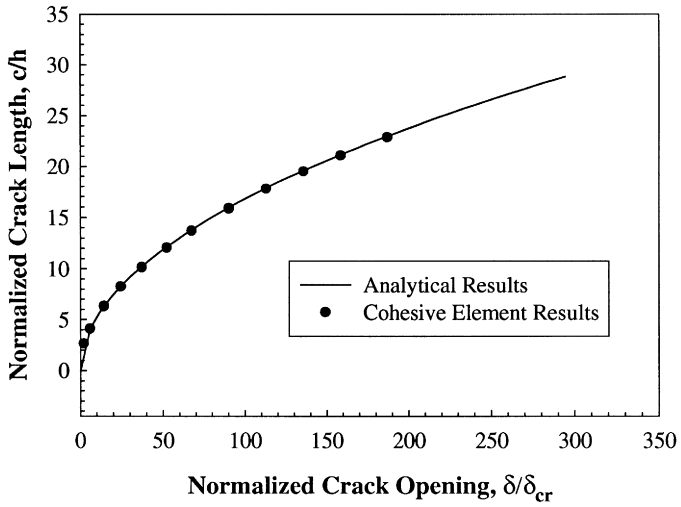

Fig. 4. Comparison between analytical and computational results for crack propagation in an elastic DCB specimen.

4. Peel analysis

Consider a peel test as shown in Fig. 5. The fracture toughness of the interface, Γ_0, energy dissipation in the peel arm, and external work are related by an energy balance for the entire system (Kinloch, 1987). For an incremental crack advance, dx, the external work done by the loading, $(1-\cos\varphi)F\,\mathrm{d}x$, equals the sum of the change in elastic energy stored in the peel arms, $\mathrm{d}W^{\mathrm{e}}$, the work expended as dissipation in the peel arms, $\mathrm{d}W^{\mathrm{v}}$, and the energy spent in interface separation, $\Gamma_0 w\,\mathrm{d}x$, i.e.,

$$(1-\cos\varphi)F\,\mathrm{d}x = \mathrm{d}W^{e} + \mathrm{d}W^{v} + \Gamma_0 w\,\mathrm{d}x \tag{18}$$

The term $\mathrm{d}W^{\mathrm{e}}$ is commonly neglected since during experiments steady state peeling is obtained with the aid of a stiff backing material attached to the polymer. Written in this form, eqn (18) suggests that the terms $\mathrm{d}W^{\mathrm{v}}$ and Γ_0 are uncoupled, and have been treated as such in several analyses discussed in the Introduction.

If a steady state exists, there is no change in the shape of the peel arms in an incremental sense. When there is no change in the elastic strain energy, $\mathrm{d}W^{\mathrm{e}}$, the work done by the external loads on the system is the experimentally measured fracture energy, Γ, i.e.,

$$\Gamma = \frac{1}{w}(1-\cos\varphi)F = \Gamma_0 + \frac{1}{w\,\mathrm{d}x}\mathrm{d}W^{\mathrm{v}} \tag{19}$$

This is the sum of the fracture toughness of the interface and the energy dissipated in the peel arm.

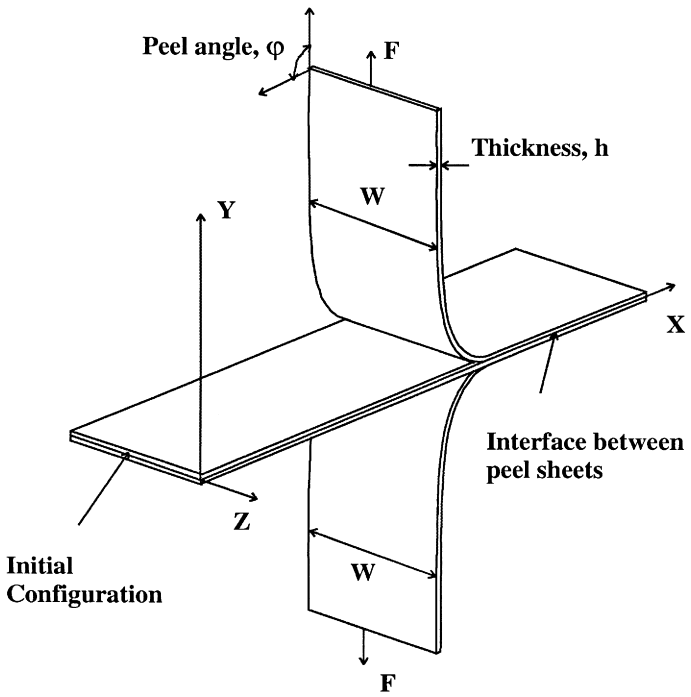

Fig. 5. Geometry of a peel test.

4.1. Dimensional analysis

Consider a peel test shown schematically in Fig. 5, where the material in the peel arms is characterized as a linear viscoelastic solid. Assume that the bulk modulus is a fixed number; all the relaxation then occurs in shear deformation. The cohesive zone is characterized by two rate-independent parameters, Γ_0, and δ_{cr}. The geometrical parameters that define the peel geometry are the thickness, h, and width of the peel, w. Loading in the problem is specified as the peeling force per unit width of the peel, F/w, and the peel velocity, V.

We present a dimensional analysis that helps to organize these variables into dimensionless groups. Similar dimensional analyses have been considered earlier in the literature by Tvergaard and Hutchinson (1992) for fracture in elastic–plastic solids, and by Carpinteri (1991) in the study of size scale transition from ductile to brittle failure. Consider first the case where the material properties may be represented by the standard linear solid. The complete list of parameters that characterize the peeling process are:

$$\begin{aligned} &G_\infty, G_0, \tau_0 && \text{standard linear solid properties}\\ &\Gamma_0, \delta_{cr} && \text{fracture process}\\ &h, V, F/w, \varphi && \text{geometry and loading} \end{aligned} \tag{20}$$

where τ_0 is the relaxation time of the standard linear solid. A dimensional analysis reveals that the force per unit width in a peel test, $(1-\cos\varphi)F/w = \Gamma$, is related to a combination of dimensionless parameters in a functional form, Φ, given as

$$\Gamma = (1-\cos\varphi)\frac{F}{w} = \Gamma_0\Phi\left(\frac{G_\infty}{G_0}, \frac{G_0 h}{\Gamma_0}, \frac{\tau_0 V}{h}, \frac{\delta_{cr}}{h}\right) \tag{21}$$

Γ scales with intrinsic toughness Γ_0. However, it also depends on other parameters. The dimensionless parameter, $\lambda = G_\infty/G_0$, characterizes the viscoelastic rheology of the material in the peel arms and the dimensionless parameter, $G_0 h/\Gamma_0$, couples the fracture energy of the interface with the thickness of the peel arm and short time modulus. The parameter, $V^* = \tau_0 V/h$, can be interpreted as the ratio of the relaxation time of the polymer to that of the time required to propagate the crack tip along the interface by a distance equal to the peel thickness.

It is well known that the bulk material properties of many polymers satisfy a rate-temperature equivalence principle based on a shift parameter, a_T, that is defined by the Williams, Landel, Ferry (WLF) equation (Ferry, 1980) as

$$\log_{10}(a_T) = \frac{-C_1(T-T_g)}{C_2 + (T-T_g)} \tag{22}$$

where T_g is the glass-transition temperature of the material. For many 'ideal' rubbers constants C_1 and C_2 take the values 17.4 and 51.6, respectively. The time constant, $\tau_0(T)$, for any temperature T is then given by the relation $\tau_0(T) = a_T(T)\tau_0(T_g)$. Thus the non-dimensional form, $\tau_0(T)V/h$, at a temperature, T, can be written as $\tau_0(T_g)[a_T(T)V]/h$. Therefore, the functional form, Φ, for the growth in the fracture energy, Γ, is a function of the reduced peel velocity, $a_T(T)V$. Consequently, the dependence of peel energy on rate and temperature exhibits rate-temperature equivalence similar to that demonstrated by the bulk properties of the polymer sheets. The parameter, (δ_{cr}/h), normalizes the critical opening displacement of the cohesive zone with the other length scale present in the problem at steady state,

namely the thickness of the peel arm. The above functional form for the fracture energy can be split into two parts, Γ_0 and $\Gamma_0(\Phi - 1)$, resulting in a form consistent with the empirical eqn (1). The dimensional analysis is readily generalized to the case when the material is represented by a generalized Maxwell series eqn (12) as

$$\Gamma = \Gamma_0 \Phi\left(\frac{G_\infty}{G_0}, \frac{G_i h}{\Gamma_0}, \frac{K_\infty}{K_0}, \frac{K_j h}{\Gamma_0}, \frac{\tau_i^G V}{h}, \frac{\tau_i^k V}{h}, \frac{\delta_{\mathrm{cr}}}{h}\right) \tag{23}$$

where $i = 1, \ldots, n_G, j = 1 \ldots n_K$,

$$G_0 = G_\infty + \sum_{i=1}^{n_G} G_i, \quad \text{and,} \quad K_0 = K_\infty + \sum_{i=1}^{n_k} K_i.$$

4.2. Elastic peel analysis

A large deformation elastic T-peel test problem ($\varphi = 90^\circ$) with material properties that are characteristic of a fully relaxed polymer is used to study elastic peeling. The elastic T-peel test problem is shown schematically in Fig. 5. It serves as an important limiting case of the viscoelastic analysis. It also allows one to verify that the model computes a steady state value of peel force which, for an elastic material, depends only on the intrinsic cohesive energy Γ_0, and not on other cohesive zone parameters.

A schematic of the finite element mesh for the computational model of an elastic T-peel test is shown in Fig. 3. Invoking symmetry about the x–z plane, we model only the upper half. Geometric and materials parameters are: length $L = 0.1$ m, thickness $h = 0.001$ m, bulk modulus, $K = 5$ GPa, shear modulus, $G = 1$ MPa, and cohesive zone fracture energy $\Gamma_0 = \phi_{\mathrm{n}} = \phi_{\mathrm{t}} = 10.0$ J/m^2. The problem is analyzed for two different values of the critical opening displacements, $\delta_{\mathrm{cr}} = \delta_{\mathrm{n}} = \delta_{\mathrm{t}} = 50$ and 500 μm. The bulk is discretized by four-node hybrid plane strain elements with incompatible mode shape functions. These elements are based on a mixed displacement-pressure formulation. Four-node cohesive elements placed along the axis of symmetry are used to model the interface. The normalized size of the cohesive elements, $\Delta_{\mathrm{h}}/\delta_{\mathrm{cr}}$, for the two different δ_{cr} are 2.5 and 0.25, respectively. Displacement constraints include coupling of the cohesive element nodes to account for symmetry are similar to those used for the elastic DCB problem. It is customary in experimental peel tests to provide a quasi-rigid backing on the peel material to avoid large axial stretching and to attain a steady state. Spring elements placed on the peel surface at $y = h$, as shown in Fig. 3, are used to model such a backing. The spring elements are active only in tension and do not offer any resistance in compression. The force–axial strain relationship in tension for the spring elements is given by the nonlinear relation

$$P = \alpha\left(\frac{\varepsilon}{\beta}\right)^n \tag{24}$$

where $n = 2$, and $\beta = 0.001$ is a characteristic strain. The coefficient α is chosen such that the axial stiffness of the springs, given by $\mathrm{d}P/\mathrm{d}\varepsilon$, is equal to ten times the shear modulus of the elastic peel at a strain level of $\varepsilon = \beta$. This form of relation for the force–axial strains in the springs provides axial rigidity that increases linearly with the straining of springs.

The elastic beam element is used as a loading mechanism to obtain a 90° peel angle. Loading is applied in two steps. The first step consists of a prescribed 90° rotation along the negative z-axis to the two end nodes of the beam element along with a specified peel rate in the form a nodal velocity, $V = 1.0 \times 10^{-9}$ m/s, to the node located at $x = 0$, $y = h$. In the second step, the angle is held constant while the nodal velocity continues to act until a steady state is reached.

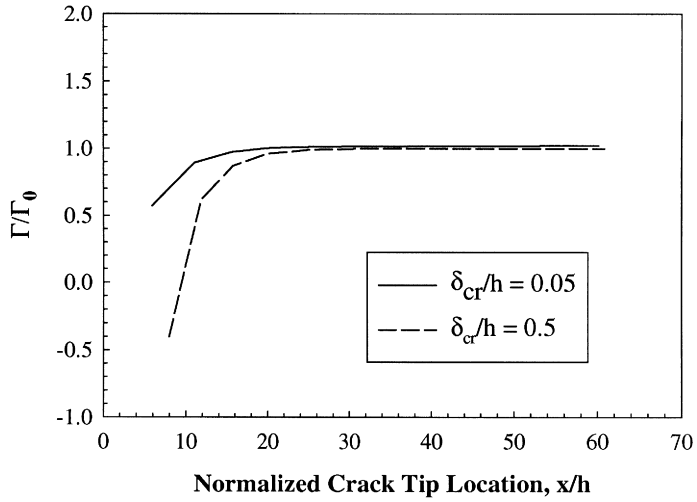

Fig. 6. Evolution of fracture energy to steady state in elastic peeling.

A plot of the deformed shape at steady state is shown in Fig. 5. The bottom peel is obtained by reflecting the modeled top half. The evolution of normalized fracture energy, Γ/Γ_0, with crack advancement in the elastic peeling process is shown in Fig. 6. At steady state the work done on the system reaches a steady value which, as measured by the peel force, is achieved when the crack advances by about twenty peel thicknesses (h) along the interface. As expected, the steady state value for Γ is independent of the magnitude of δ_{cr} used in the analysis. An analysis without the spring elements leads to results that are numerically indistinguishable from these results.

4.3. Viscoelastic peel analysis

4.3.1. Problem formulation

Consider again Fig. 5 where the peeling material is now viscoelastic. For the results presented in this section, it is taken to be a standard linear viscoelastic solid. The material is assumed to have no relaxation in the bulk behavior; all the relaxation occurs in shear deformation. The bulk and shear moduli as a function of time are given as

$$K(t) = K$$

$$G(t) = G_\infty + (G_0 - G_\infty)\exp\left(-\frac{t}{\tau_0}\right) \tag{25}$$

This is identical to a one-term generalized Maxwell series representation for the shear modulus with a single relaxation time, τ_0, and a constant bulk modulus. The numerical values employed in this study are $K = 5$ GPa, $G_0 = 10$ MPa, $G_\infty = 1$ MPa, and $\tau_0 = 1.0$ s. The ratio, $G_\infty/G_0 = 0.1$, is chosen to obtain a steady state by the time the crack tip propagates by 40–60 times the peel thickness. For smaller ratios, a longer peel length is required to reach steady state.

A set of dimensionless parameters for convenience in understanding and interpretation of the analysis results are defined as

$$\lambda = \frac{G_\infty}{G_0}$$

$$V^* = \frac{\tau_0 V}{h}, \quad V_h = \frac{h}{\tau_0}$$

$$\Gamma^* = \frac{\Gamma}{\Gamma_0}$$

$$\sigma_{\mathrm{n}}^* = \frac{T_{\mathrm{n}}}{\sigma_{\mathrm{cr}}}$$

$$\Delta^* = \frac{\Delta \mathrm{h}}{\delta_{\mathrm{cr}}} \tag{26}$$

V_{h} is a characteristic peel velocity and V^* is the ratio of the peel velocity to the characteristic velocity V_{h}.

4.3.2. Predictions of fracture toughness

We present first two cases of the peel problem with the same dimensionless parameters in the function Φ in eqn (21). The parameters used for these cases are: Case 1: $\Gamma_0 = 10$ J/m^2, $h = 1.0$ mm, $\Delta_{\mathrm{h}}/\delta_{\mathrm{cr}} = 2.5$,$\delta_{\mathrm{cr}} = 50\ \mu$m; and Case 2: $\Gamma_0 = 5$ J/m^2, $h = 0.5$ mm, $\Delta_{\mathrm{h}}/\delta_{\mathrm{cr}} = 2.5$, $\delta_{\mathrm{cr}} = 25\ \mu$m. The peel analysis is performed for varying normalized peel velocities, V^*. A plot of the deformed shapes of the peel at steady state for three representative velocities (low, medium and high) are shown in Fig. 7(a, b, c), respectively. In the limiting cases of low and high velocities the material behaves elastically everywhere and the curvature decreases monotonically to zero from a maximum value at the crack tip. At low velocities, the material is completely relaxed to the lower modulus G_∞ causing the peel arm to have larger curvature, overall, while at high velocities the material is stiff as it is unrelaxed at G_0 causing the peel arm to deform with a smaller curvature. At medium velocities, with increasing distance from the crack tip, the curvature reduces, changes sign, and ultimately approaches a limiting value of zero. This results from the viscoelastic nature of the material that causes different parts of the peel arm to exhibit different incremental stiffness. Similar shapes for peel arms in the peeling of viscoelastic sheets were obtained by Kendall (1972).

The variations in the normalized fracture energy, Γ^*, with normalized velocity, V^*, for the two cases considered are shown in Fig. 8. The two plots are identical within computational accuracy, verifying the dimensional analysis presented in Section 4.1. This also further verifies the assertion that the fracture energy scales with the intrinsic fracture toughness at a fixed velocity. Thus, the viscous dissipation in the peel arm is not independent of the intrinsic fracture toughness of the interface, consistent with eqn (1). Consider now the three different regimes drawn in Fig. 8 corresponding to the low, medium and high normalized velocities V^*. In the low and high velocity regimes fracture energy equals the intrinsic fracture energy. In the medium velocity regime the fracture energy and viscous dissipation in the peel arm are sensitive to the normalized peel velocity, V^*, and attain a maximum. An upper bound on the fracture energy can be obtained by considering the case of a crack propagating in an infinite medium characterized by the linear solid material properties. It is known for this case that the maximum possible fracture energy equals Γ_0/λ (Hui et al., 1992). For the case of a peel with finite thickness there is a limit on the size of the viscous dissipation zone (Fig. 1) and hence it is expected the maximum normalized fracture energy, Γ^*, can be smaller than $1/\lambda$. For the material properties considered here $1/\lambda$ evaluates

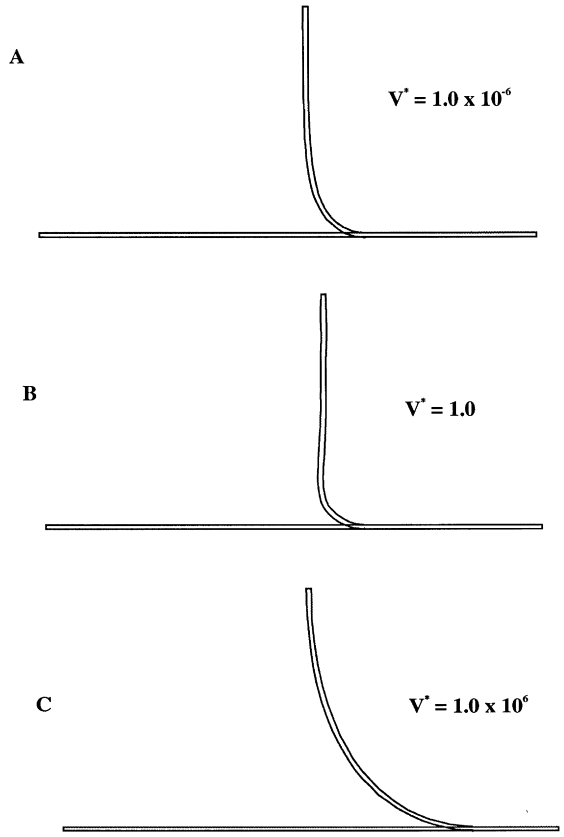

Fig. 7. (a, b, c). Viscoelastic peel deformed shapes at low, medium, and high peel velocities.

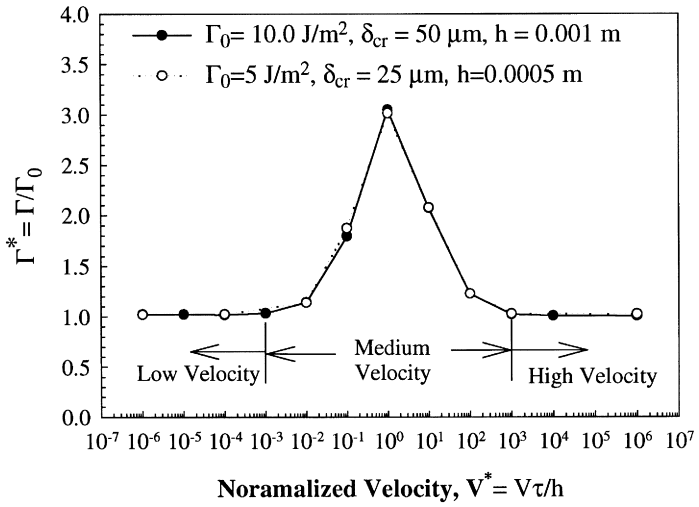

Fig. 8. Variation of fracture energy, Γ^*, with the normalized velocity, V^*.

to 10 and from Fig. 8 it is observed that numerical modeling predicts a factor of about 3. The variation of the cohesive zone size at steady state is shown in Fig. 9 for varying normalized peel velocities. The cohesive zone size attains limiting values in the low and high velocity regimes. The increase in cohesive zone size with velocity is consistent with the increased stiffness of the material. A soft peel arm in the low velocity regime, as seen from Fig. 7(a), results in a smaller cohesive zone whereas a stiffer unrelaxed peel arm in the high velocity regime, as seen from Fig. 7(c), results in a larger cohesive zone. However, in the transition between the two limits there is an overshoot; the largest cohesive zone is at an intermediate velocity.

Qualitatively, the shape shown in Fig. 7(b) and the fact that the largest cohesive zone size occurs at an intermediate velocity may be understood as follows. Imagine a material with stiffness, G_0, everywhere which has a characteristic peel shape. Imagine now that a portion of the peel arm, say from the point of load application to some distance behind the crack tip, is relaxed to the rubbery modulus G_∞. Because the stiff material just behind the crack tip is now attached to the point of load application by a soft peel arm, the shape will now change to a lower curvature near the crack tip with an associated increase in cohesive zone length.

A measure of the transition region where viscous dissipation is localized can be obtained by plotting a parameter ρ along the peel arm. The parameter ρ is defined as

$$\rho = \frac{\varepsilon - \varepsilon_0}{\varepsilon_\infty - \varepsilon_0} \tag{27}$$

where $\varepsilon = \sqrt{2/3\mathbf{e}:\mathbf{e}}$, and $\mathbf{e}$ is the total deviatoric strain. This parameter was proposed and used by Hui et al. (1992) to depict the viscous dissipation zone near a crack tip under small-scale yielding. The quantities, ε_0 and ε_∞, are obtained by dividing the actual Mises stress at the material point by three times the unrelaxed shear modulus, G_0, and the fully relaxed shear modulus, G_∞, respectively. In the

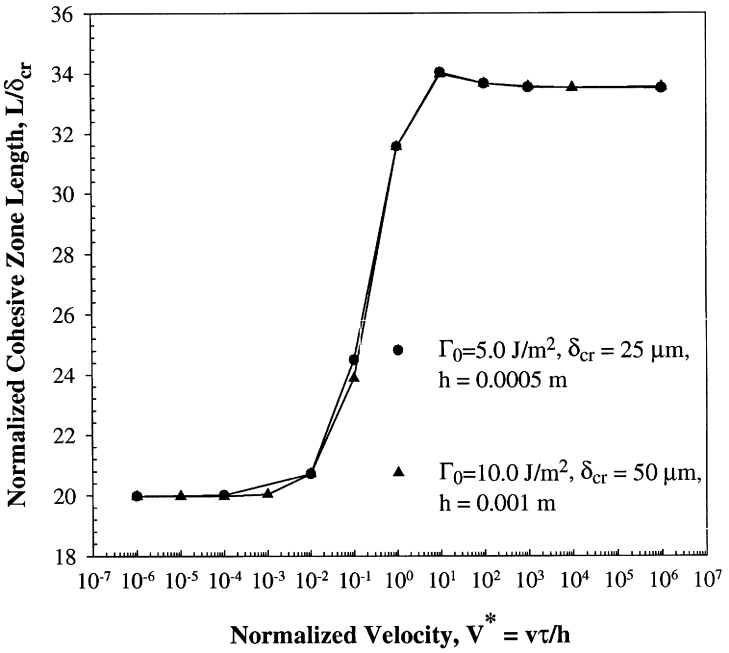

Fig. 9. Variation of cohesive zone size with peel velocity.

completely relaxed and completely unrelaxed states the parameter, ρ, would be close to 1.0 and 0.0, respectively. A value of the parameter, ρ, away from either 1.0 or 0.0 indicates departure from linear elasticity, i.e., it indicates viscous deformation. The distribution of the parameter ρ evaluated along the tensile fiber of the peel arm is shown in Fig. 10 for a number of peel velocities. These plots correspond to $\Gamma_0 = 10$ J/m^2, $\delta_{cr} = 50$ μm, and $h = 1$ mm. The origin of the x-axis of the plot is located at the crack tip, x_c. For $V^* \ll 1$ the polymer sheets are completely relaxed everywhere to their long term modulus, G_∞. There is little dissipation and we expect the parameter ρ to be close to 1.0 as is evident from Fig. 10. For $V^* \gg 1$, the crack is travelling in an unrelaxed elastic material with shear modulus, G_0. The parameter, ρ, as expected, is close to zero everywhere. For intermediate velocities, $V^* \approx O(1)$, or the peel velocity, $V \approx V_h$, the material will relax from an initially stiff state as it enters the cohesive zone to a soft state as behind the crack tip. Plots of the variation in parameter, ρ, along the peel arm for $V^* = 0.1$, 1.0 (peak dissipation), and 10.0 are also shown in Fig. 10. At the velocity corresponding to peak dissipation, there is a distinct peak in ρ some distance behind the crack tip. The region of viscous dissipation has detached from the crack tip and moves further behind with increasing velocity.

It is useful to compare the results obtained above with those obtained by Xu et al. (1992), who study the problem of a crack propagating along the interface of two bonded viscoelastic polymer sheets modeled as a standard linear viscoelastic solid in a DCB geometry. Using a rate-independent Dugadle-like constant stress cohesive zone model they derive results for macroscopic fracture energy of the form

$$\Gamma = \Gamma_0\left[1 + \phi(v^*, c)\right] \tag{28}$$

where $v^* = \tau_0 V/a\lambda$, $c = (E_0 I \delta_{cr})/(2a^4\sigma_c)$. The parameter, a, is the horizontal distance between the point of application of load and the crack tip; E_0 is the short term Young's modulus; I is the moment of inertia; and σ_{cr} is the constant failure stress of their cohesive zone model. We evaluate eqn (28) using

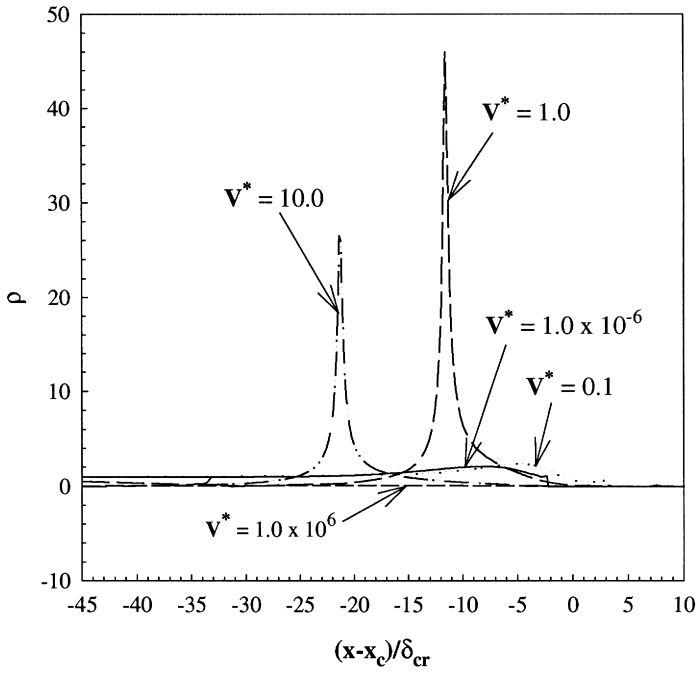

Fig. 10. Plots of parameter, ρ, representing regions of viscous dissipation along the peel arm for various peel velocities.

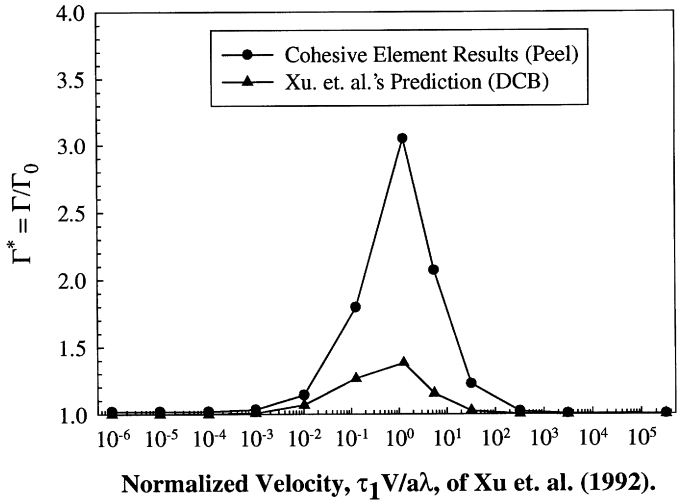

Fig. 11. Comparison of the fracture energy as predicted by the cohesive element computational model (peel) and the Xu et al. (1992) model (DCB).

values for parameters, a and c, from the present peel finite element analysis, using δ_{cr} as defined here, and $\sigma_c = \sigma_{max}$ of the Xu and Needleman cohesive zone model eqn (17). The resulting values are compared against the fracture energies as obtained from the present computational model in Fig. 11. Peel analysis computes a peak fracture energy that is considerably higher than in an equivalent DCB specimen. This itself is not remarkable considering the difference in geometry. We do find that the velocity at which peak dissipation occurs as predicted by the present computational framework and the DCB model are approximately the same. This suggests that the location of the viscous dissipation zone with respect to the finite specimen geometry is similar in the two cases.

4.3.3. Effect of cohesive zone model parameters

Observe from eqn (21) that Φ may depend on the cohesive zone parameters, δ_{cr} and Γ_0, apart from the viscoelastic properties of the polymer sheets, λ, and the sheet thickness, h. As mentioned earlier, for linear elastic solids, the parameter, Γ_0, alone is sufficient to characterize crack propagation; the critical energy release rate and cohesive zone approaches coincide in the limit $\delta_{cr} \to 0$. For models of the elastic peel test, even the condition $\delta_{cr} \to 0$, may be relaxed. As long as steady state is achieved, peel energy equals Γ_0. As pointed out by Rice (1978), for cracks in a viscoelastic material, the cohesive zone approach to crack propagation differs from one based on critical energy release rate. The implication for modeling with cohesive elements is that at least two parameters, Γ_0 and δ_{cr}, must be specified, even if it is accepted that the detailed shape of the cohesive law is unimportant. Together, through eqn (16), they specify a charteristic maximum stress in the cohesive zone.

Simulations have been conducted for a range of peeling velocities at a specified intrinsic fracture energy, $\Gamma_0 = 10$ J/m^2, peel thickness, $h = 1.0$ mm, and for three values of δ_{cr}, namely, 50, 250, and 1250 μm. Results for normalized fracture energy, Γ^*, as a function of normalized peeling velocity, V^*, are shown in Fig. 12. Again, fracture energies are independent of δ_{cr} in the two limits, $V^* \gg 1$ and $V^* \ll 1$, and are equal to the intrinsic fracture energy, Γ_0. The parameter, δ_{cr}, has considerable influence on the predicted peak in the fracture energy for the same viscoelastic material properties of the polymer sheets. With decreasing δ_{cr} the predicted fracture toughness begins to grow and peaks at lower velocities. Predicted fracture energies fall rapidly to the right of the peak values and this part of the curves is less

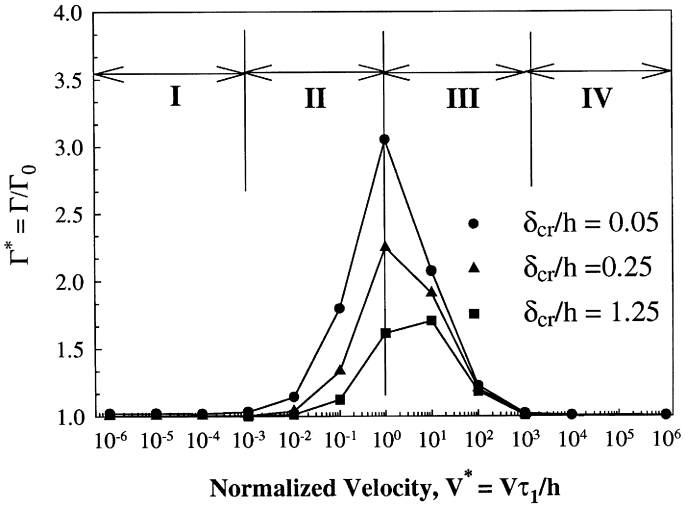

Fig. 12. Effect of critical opening displacement on fracture energy.

sensitive to changes in δ_{cr}. Thus, the low velocity and medium velocity zones shift to the left on the normalized velocity scale while the high velocity zone is relatively insensitive to δ_{cr}.

The results of Fig. 10 and 12 may be interpreted in terms of the de Gennes (1996, 1997) and Hui et al. (1992) picture of viscoelastic fracture (Fig. 1):

1. The material is elastic everywhere with relaxed rubbery modulus, $v\tau/\lambda < L$ (cohesive zone size). Peel energy is insensitive to δ_{cr}.
2. The viscous region develops, $v\tau/\lambda > L$, but the glassy region has not developed, $v\tau < L$. Peel force is sensitive to δ_{cr}.
3. The material near the cohesive zone is elastic with the glassy modulus, $v\tau > L$. Peel force is relatively insensitive to δ_{cr}.
4. The material is elastic everywhere with the glassy modulus, $v\tau > a$ (peel length). Peel force is insensitive to δ_{cr}.

Decreasing δ_{cr} implies decreasing L, although the relationship between the two is not simple. With decreasing δ_{cr} the transition from region I to II occurs at decreasing velocities, consistent with the condition for transition between the regions $v\tau/\lambda > L$. In region III, $v\tau > L$; the region of energy dissipation detaches from the cohesive zone which is surrounded by an elastic region with modulus G_0. Consequently, the peel energy again depends only on Γ_0, not on δ_{cr}. Normalized tractions along the fracture surface are shown in Fig. 13 as a function of distance from the crack tip at peak dissipation for three different values of δ_{cr}. Maximum cohesive zone traction scales inversely with δ_{cr}. The cohesive zone size decreases with decreasing δ_{cr}. However, because of accompanying changes in the peel shape the reduction in cohesive zone size is not proportional to δ_{cr}.

In the limit, $\delta_{cr} \to 0$, the cohesive zone and energy release rate approaches to viscoelastic fracture are again equivalent (Rice, 1978). In this limit the fracture process is controlled by only one cohesive zone parameter, Γ_0. In the present analysis, for $\Gamma_0 = 10$ J/m^2 and $\delta_{cr} = 1250$ μm we obtain $\sigma_{max} = 0.003$ MPa, $L = 4800$ μm, $\Gamma = 17.0$ J/m^2; and for $\Gamma_0 = 10$ J/m^2 and $\delta_{cr} = 5$ μm we obtain $\sigma_{max} = 0.7$ MPa, $L = 300$ μm, $\Gamma = 45.0$ J/m^2. Whether a limit in which only Γ_0 needs to be specified is achievable with physically acceptable values of δ_{cr} can be examined by studying the dependence of cohesive zone size, L, on the dimensionless number 'c', eqn (28). Fig. 14 plots cohesive zone size as a function of this number. It

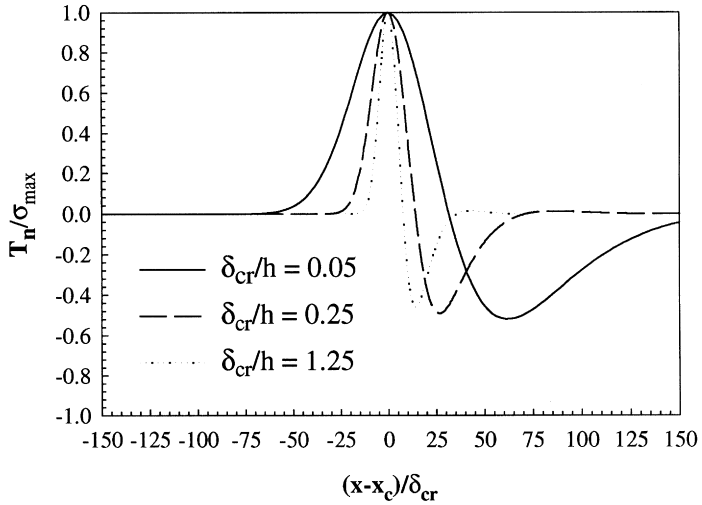

Fig. 13. Variation of tractions along the length of the peel arm at steady state for velocities resulting in peak dissipation.

includes results from the present analysis and those of Xu et al. (1992). For a given set of material properties and thickness of the polymer sheets, and intrinsic fracture energy Γ_0, the parameter c is proportional to δ_{cr}^2/a^4. For small enough values of δ_{cr} we find a limit in which cohesive zone size is independent of δ_{cr}. However, for the geometry analyzed here, this is achieved only when $\delta_{cr}<1$ nm. For $\Gamma_0 = 50$ J/m^2, this would result in maximum cohesive zone tractions of about 18 GPa, much larger than the glassy modulus. We conclude, therefore, that a meaningful use of cohesive zone models for modeling fracture in viscoelastic materials requires the knowledge of one additional parameter, namely either δ_{cr} or σ_{max}, apart from the intrinsic energy of the interface, Γ_0.

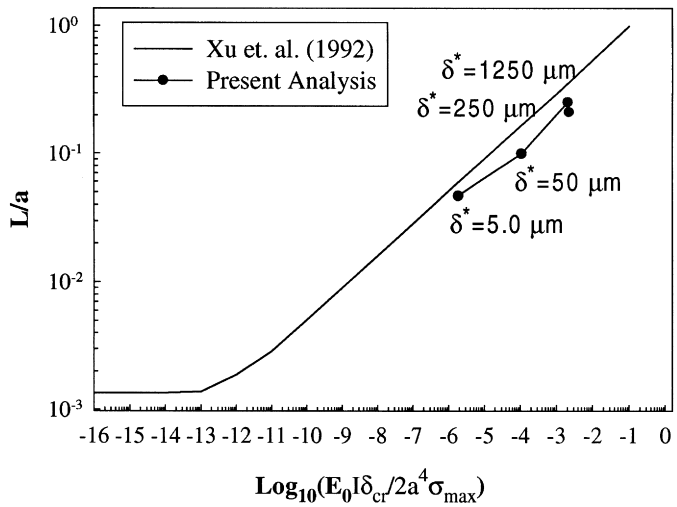

Fig. 14. Variation of the cohesive zone size with critical opening displacement.

5. Peeling of polybutadiene elastomer sheets

Consider now the well-known results on peeling of polybutadiene elastomers (Chang, 1980; Gent, 1996). The peel energy is considered qualitatively to be a combination of a rate-independent intrinsic work of fracture and viscoelastic losses in the bulk. Observed increases in peel energy with peel velocity are attributed to bulk viscoelastic losses. Here we employ the model developed to test this hypothesis quantitatively.

For a controlled level on interfacial cross-linking, the threshold strength of self adhesion, the intrinsic fracture toughness of the interface, Γ_0, was determined by Chang (1980) at high test temperatures and low rates of peeling, conditions under which viscoelastic dissipation effects are minimized. Peel energy for a set of higher rates of peeling at various test temperatures above the glass transition temperature of the elastomer were also measured. The peel rates at these various test temperatures were converted to a reduced peel rate scale which was obtained by multiplying the actual peel rates by the corresponding WLF shift factor, a_T (Ferry, 1980), calculated for the difference in the test temperature and glass transition temperature of the elastomer. The fracture energies when plotted as a function of these reduced peel rates fell on a single curve. Detailed mechanical characterization of the elastomer in the form of the tensile dynamics properties was also given in the reference, Chang (1980).

Plots of the storage and loss moduli, E' and E'', are shown in Fig. 15 as a function of the reduced frequency, ωa_T, Chang (1980). These were transformed into the transient Young's modulus through the use of equations relating the dynamic components to the transient modulus (Ferry, 1980). The resulting transient Young's modulus was converted to transient shear modulus by using the relation, $G(t) = E(t)/(2(1+\upsilon))$. A value of 0.5 was used for Poisson's ratio, υ, in this relation. An eight-term Generalized Maxwell series fit, as in eqn (12), was obtained for the transient shear modulus data. The normalized generalized Maxwell series coefficients, $g_i = G_i/G_0$, and the corresponding relaxation times from this fit are listed in Table 1. A plot of the experimentally obtained transient shear modulus and the Generalized Maxwell series approximation is shown in Fig. 16. The glassy modulus for the elastomer, G_0, was not provided; it was assumed to be 1.0 GPa. As will be evident presently, the main conclusions here are not sensitive to the quality of the fit to viscoelastic measurements in the glassy region as through most of the time and temperature regime being analyzed the material is close to being in the rubbery state. It is assumed that there was no relaxation in the volumetric deformation of the elastomer, and the bulk modulus, K, was chosen as 2.0 GPa.

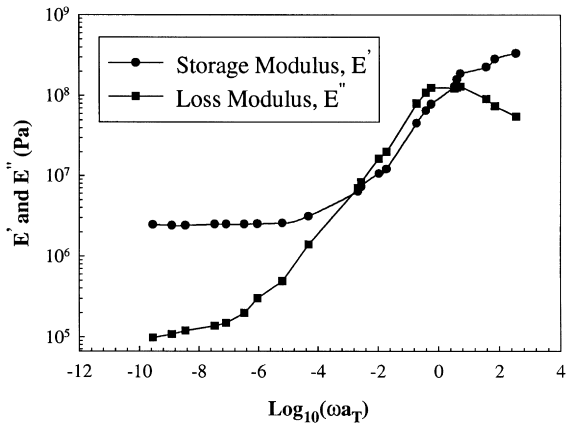

Fig. 15. Storage and loss modulus for a butadiene elastomer (Chang, 1980).

Table 1
Generalized Maxwell series coefficients and relaxation times for the butadiene elastomer at its glass-transition temperature, −90°C

Term no., i	Normalized shear modulus $G_i = G_i/G_0$	Time constant τ_I^G (s)
1	0.88392	3.56484E-3
2	3.41887E-2	2.85973E-2
3	2.51032E-2	0.26090
4	2.82918E-2	1.5327
5	1.77887E-2	9.6884
6	7.30381E-3	84.922
7	2.14218E-3	1467.9
8	4.90413E-4	1.62799E+5

The table is based on data of Chang (1980).

The specimen for the T-peel test in the experimental investigation had the following dimensions: peel thickness, $h = 0.75$ mm, length of the peel, $L = 80$ mm. The experimental investigation used a cotton cloth attached to the top of the specimen to minimize large extensions. As described in Section 4.3.1, spring elements with the force–elongation relationship in tension only, as given by eqn (24), were used to model the cotton cloth. The work of intrinsic fracture energy, Γ_0, for the cohesive elements was assumed to be equal to the threshold strength of self adhesion of the elastomer measured at high temperature and low peel velocity. One such threshold work of self-adhesion for the BR elastomer was measured to be 22.5 J/m^2. The critical opening displacement, δ_{cr}, for the cohesive elements is taken as 50 μm.

A plot showing the experimentally measured growth in peel energy with the reduced peel rate is shown in Fig. 17. The numerical simulations were carried out for a range of peeling rates from 10^{-13} to 10^{-4} m/s. It is observed that the numerical results using a rate-independent cohesive zone model predict onset of viscous dissipation only above 10^{-9} m/s. Experimental measurements reveal that viscous dissipation begins at the peel velocities on the order of 10^{-19} m/s: an immense discrepancy of about 10 orders of magnitude. The experimentally observed growth in fracture energies at velocities as low as 10^{-19} m/s needs to be commented upon. Attention is drawn to the comments of Gent (1996) on this

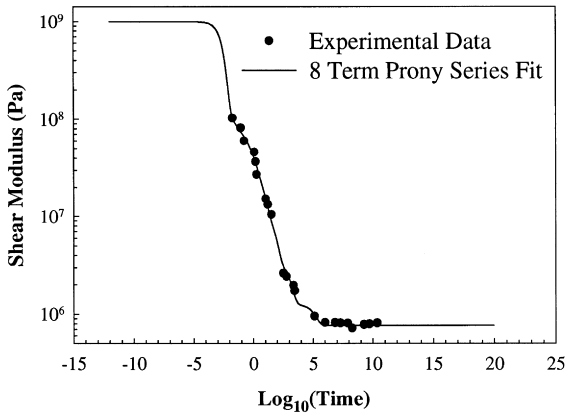

Fig. 16. Dynamic shear modulus for butadiene elastomer and a generalized Maxwell series fit.

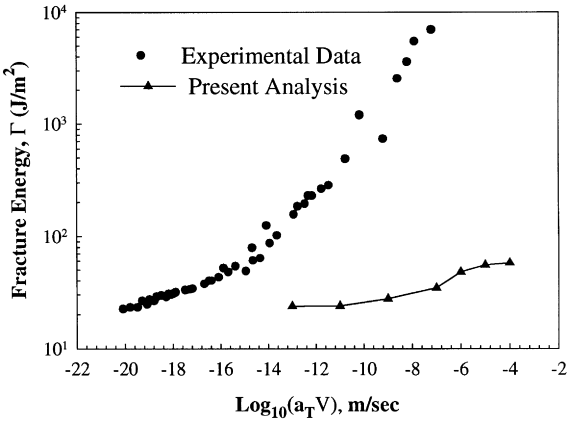

Fig. 17. Experimental fracture energy and cohesive zone model predictions.

point. Based on the largest relaxation time in the Maxwell series fit, $\tau = 1.5 \times 10^5$ s, at these rates $v\tau \approx 10^{-14}$ m and $v\tau/\lambda \approx 10^{-11}$ m. In other words, the glassy and viscous zones of Fig. 1 have not appeared and the rubbery zone extends throughout the material. These rates are too low for appreciable viscous dissipation to develop in the peel arm. Based on the discussion in the previous section, detailed predictions will depend on the actual choice of δ_{cr}. However differences due to changes in δ_{cr} are too small to account for the large discrepancy between theory and experiment.

We suggest, instead, that the observed growth in the fracture energy at such small velocities be modeled by rate-independent dissipation in the intrinsic fracture zone, which would manifest in the model as a rate-dependent cohesive zone model. As mentioned in the Introduction, several authors have developed and used rate-dependent models in other contexts. However, this finding and suggestion goes against the usual interpretation of viscoelastic peeling data (Gent, 1996; de Gennes, 1996) that the total dissipation consists of a rate-independent work of separating the cohesive zone coupled multiplicatively to viscoelastic dissipation in the bulk. Whether these data can be modeled quantitatively with an appropriate rate-dependent cohesive law remains to be established and is the focus of ongoing work.

6. Conclusions

A computational framework for modeling fracture propagation in viscoelastic materials has been developed. The development accounts for geometric nonlinearities and allows for the formation of macroscopic crack surfaces through the use of a cohesive zone model implemented using a cohesive surface finite element. The developments are used to study the growth in viscoelastic losses and fracture energy in the peeling of a linear viscoelastic material. A dimensional analysis of the peel test problem shows that peel energy is proportional to Γ_0. It also depends on other geometrical and material parameters. Computed results verify the dimensional analysis and the functional form for the relationship between peel energy and peel velocity. This conclusion is in contrast to several earlier peel analyses where it was assumed that viscous dissipation in the peel is independent of the intrinsic fracture energy of the interface.

Analysis of peeling of a material represented by the standard linear solid shows that viscous dissipation is negligible at peel rates that are small and large compared to a characteristic peel velocity, V_h, which depends on the specimen geometry and relaxation time. In these limits, peel energy equals the intrinsic interfacial energy. Between the two limits, with increasing peel velocity, peel energy increases,

attains a peak value, and decreases to the intrinsic interfacial toughness. Various regimes in peeling velocity have been interpreted in terms of de Gennes (1996, 1997) picture of different zones near a crack propagating in a viscoelastic material. We find that to model accurately the regime of velocities below peak dissipation it is necessary to specify at least two cohesive zone parameters, e.g., δ_{cr} and Γ_0. In this regime the viscous dissipation region engulfs the cohesive zone. In the regime of velocities above peak dissipation the viscous dissipation region detaches from the cohesive zone. The cohesive zone is surrounded by an elastic region and can now be described by a single parameter, e.g., Γ_0.

The computational model, when used to model experimental peel tests on Butadiene elastomers, reveals that the predicted increase in peel energy occurs at much larger peel velocities compared to experiment. Analysis of velocities at which experiments show viscous dissipation results in a viscous dissipation zone on the order of 10^{-11}m. This has also been pointed out by Gent (1996) who suggests local crack branching as a source of energy dissipation. Within the context of a continuum model it is suggested that these experiments be analyzed using a rate-dependent cohesive zone model. Such suggestions have also been made in literature earlier for modeling fracture in concrete by Carpinteri et al. (1997).

References

ABAQUS, Version 5.7, 1997. Theory and User Manuals I, II and III, Hibbitt, Karlsson, and Sorensen, Inc., 1080 Main Street, Pawtucket, R.I., 02860-4847, USA.

Ahagon, A., Gent, A.N., 1975. Effect of interfacial bonding on the strength of adhesion. Journal of Polymer Science: Polymer Physics 13, 1285–1300.

Andrews, E.H., Kinloch, A.J., 1973. Mechanics of adhesive failure—I. Proceedings of Royal Society London A 332, 339–385.

Aravas, N., Kim, K.S., Loukis, M.J., 1989. On the mechanics of adhesion testing of flexible films. Material Science and Engineering A 107, 159–168.

Barenblatt, G.I., 1962. The mathematical theory of equilibrium cracks in brittle fracture. Advances in Applied Mechanics 7, 55–129, Academic Press.

Bazant, Z.P., Planas, J., 1998. Fracture and Size Effect in Concrete and Other Quasibrittle Materials. CRC Press, New York.

Bocca, P., Carpinteri, A., Valente, S., 1991. Mixed mode fracture of concrete. International Journal of Solids and Structures 27 (9), 1139–1153.

Camacho, G.T., Ortiz, M., 1996. Computational modeling of impact damage in brittle materials. International Journal of Solids and Structures 33 (20–22), 2899–2939.

Carpinteri, A., 1991. Size scale transition from ductile to brittle failure: structural response vs crack growth resistance curve. International Journal of Fracture 51, 175–186.

Carpinteri, A., Valente, S., Zhou, F.P., Ferrara, G., Melchiorri, G., 1997. Tensile and flexural creep rupture tests on partially-damaged concrete specimens. Materials and Structures (R.I.L.E.M) 30, 269–276.

Chang, R.J., 1980. Effect of interfacial bonding of the strength of adhesion between elastomer layers. Ph.D dissertation, University of Akron.

Chang, R.J., Gent, A.N., 1981. Effect of interfacial bonding on the strength of adhesion of elastomers—I: self-adhesion. Journal of Polymer Science: Polymer Physics 19, 1619–1633.

de Gennes, P.G., 1996. Soft adhesives. Langmuir 12, 4497–4500.

de Gennes, P.G., 1997. Soft interfaces. The 1994 Dirac Memorial Lecture. Cambridge University Press, Cambridge.

Derail, C., Allal, A., Marin, G., Tordjeman, Ph., 1997. Relationship between viscoelastic and peeling properties of model adhesives—part I: cohesive fracture. Journal of Adhesion 61, 123–157.

Dugdale, D.S., 1960. Yielding of steel sheets containing slits. Journal of Mechanics and Physics of Solids 8, 100.

Ferry, J.D., 1980. Viscoelastic Properties of Polymers, 3rd ed. Wiley, New York.

Gent, A.N., 1996. Adhesion and strength of viscoelastic solids: is there a relationship between adhesion and bulk properties? Langmuir 12, 4492–4496.

Gent, A.N., Hamed, G.R., 1977. Peel mechanics of elastic–plastic adherend. Journal of Applied Polymer Science 21, 2817–2831.

Gent, A.N., Lai, S.M., 1994. Interfacial bonding, energy dissipation, and adhesion. Journal of Polymer Science, Part B: Polymer Physics 32, 1543–1555.

Gent, A.N., Petrich, R., 1969. Adhesion of viscoelastic materials to rigid substrates. Proceedings of Royal Society London A 310, 433–448.

Gerstle, W.H., Xie, M., 1992. FEM modeling of fictitious crack propagation in concrete. ASCE Journal of Engineering Mechanics 118 (2), 416–434.

Hui, C.-Y., Xu, D.-B., Kramer, E.J., 1992. A fracture model for weak interface in a viscoelastic material (small scale yielding analysis). Journal of Applied Physics 72 (8), 3294–3304.

Kendall, K., 1972. The shapes of peeling solid films. Journal of Adhesion 5, 105–117.

Kim, K.S., Aravas, N., 1988. Elastoplastic analysis of the peel test. International Journal of Solids and Structures 24, 417–435.

Kinloch, A.J., 1987. Adhesion and adhesives: science and technology. Chapman and Hall, New York.

Kinloch, A.J., Lau, C.C., Williams, J.G., 1994. The peeling of flexible laminates. International Journal of Fracture 66, 45–70.

Knauss, W.G., 1973. On the steady propagation of a crack in a viscoelastic sheet: experiments and analysis. In: Kausch, H.H., Jaffee, R. (Eds.), Deformation and Fracture of High Polymers. Plenum Press, New York, pp. 501–541.

Knauss, W.G., 1993. Time dependent fracture and cohesive zones. Journal of Engineering Materials and Technology, Transactions of ASME 115, 262–267.

Knauss, W.G., Losi, G.U., 1993. Crack propagation in a nonlinearly viscoelastic solid with relevance to adhesive bond failure. ASME Journal of Applied Mechanics 60, 793–801.

Lake, G.J., Thomas, A.G., 1967. The strength of highly elastic solids. Proceedings of the Royal Society of London A 300, 108–119.

Lawn, B., 1993. Fracture of Brittle Solids. Cambridge Solid State Science Series. Cambridge University Press.

Loukis, M.J., Aravas, N., 1991. The effects of viscoelasticity in the peeling of polymeric films. Journal of Adhesion 35, 7–22.

Needleman, A., 1990. An analysis of decohesion along an imperfect interface. International Journal of Fracture 42, 21–40.

Ogden, R.W., 1984. Non-Linear Elastic Deformations. Ellis Horwood Limited, Chichester, England.

Rice, J.R., 1978. The mechanics of quasi-static crack growth. In: Proceedings of the Eighth U.S. National Congress on Mechanics, 191–216.

Schapery, R.A., 1975. A theory of crack initiation and growth in viscoelastic media. International Journal of Fracture 11 (1), 141–159.

Tvergaard, V., Hutchinson, J.W., 1992. The relation between crack growth resistance and fracture process parameters in elastic–plastic solids. Journal of the Mechanics and Physics of Solids 40 (6), 1377–1397.

Williams, M.L., 1963. The Fracture of viscoelastic material. In: Drucker, Gilman (Ed.), Fracture of Solids. Interscience Publishers, pp. 157–188.

Xu, D.-B., Hui, C.-Y., Kramer, E.J., 1992. Interface fracture and viscoelastic deformation in finite size specimens. Journal of Applied Physics 72 (8), 3305–3316.

Xu, X.P., Needleman, A., 1994. Numerical simulations of fast crack growth in brittle solids. Journal of the Mechanics and Physics of Solids 42 (9), 1397–1434.